Geological Society of America
Special Paper 396
2005

New insights on the origin of flow bands in obsidian

Jonathan M. Castro[†]
Department of Mineral Sciences, Smithsonian Institution, P.O. Box 37012, NMNH MRC-119, Washington, DC 20009, USA

Donald B. Dingwell
Alexander R.L. Nichols
Department für Geo- und Umweltwissenshaften, Universität München, Theresienstraße 41 III, 80333 München, Germany

James E. Gardner
Department of Geological Sciences, The University of Texas at Austin, 1 University Station C1100, Austin, Texas 78712-0254, USA

ABSTRACT

We examined the textures, volatile contents, and cooling histories of microlite-defined flow bands in several rhyolitic obsidians in order to test whether textural variations between bands could be ascribed to different degassing and cooling histories, and to assess the timing and location of band formation. Flow bands are defined by variations in microlite number density (N_V) and size. For each mineral phase examined, smaller average crystal sizes characterize the microlite-rich bands in contrast to microlite-poor bands, which contain relatively larger crystals of lower N_V. Magmatic H_2O concentrations of microlite-rich and microlite-poor bands show no statistical difference between the textures. Calorimetric measurements yield similar glass transition temperatures and cooling rates for adjacent bands. These observations suggest that microlite heterogeneities could not have developed during late stage cooling and degassing during flow emplacement, as such textural variations imply distinct cooling and/or degassing histories. Rather, textural heterogeneities must have formed during flow in the conduit.

Hydrothermal annealing experiments were conducted on natural fragmented rhyolite in order to simulate the welding process in silicate melt and to provide first-order estimates of the time scales and deformation required to produce flow bands. Flow bands formed in experiments conducted at H_2O-vapor pressures of 50 and 100 MPa, and for temperatures ranging from 800 to 850 °C. In each case, bands formed as a result of redistribution of oxide-rich domains and grain boundary coatings in annealed glass powders that underwent viscous deformation. Experiments suggest that bands may form on relatively short time scales (~7 d) and for small bulk strains (~1). Band formation may be promoted by high melt-H_2O concentrations, shear stress, and viscous and frictional heating.

Keywords: obsidian, flow banding, welding, deformation.

[†]E-mail: castro@volcano.si.edu.

Castro, J.M., Dingwell, D.B., Nichols, A.R.L., and Gardner, J.E., 2005, New insights on the origin of flow bands in obsidian, *in* Manga, M., and Ventura, G., eds., Kinematics and dynamics of lava flows: Geological Society of America Special Paper 396, p. 55–65. doi: 10.1130/2005.2396(05).

INTRODUCTION

One of the distinctive characteristics of rhyolitic obsidian lavas is the abundance of flow banding, or micrometer- to centimeter-scale structures defined by subplanar variations in microlite (crystals <100 μm) concentration (Fig. 1). As these features arise from both crystallization and deformation processes, flow bands must contain important information regarding the chemical and physical evolution of obsidian magmas. Despite their prevalence within many obsidian lavas, relatively little is known about the origins of bands. In particular, the mechanisms that generate striking variations in crystallinity, which are a prerequisite to forming bands, have only recently received attention (e.g., Tuffen et al., 2003; Gonnermann and Manga, 2003). Such information is important, for example, in defining where and when bands form. This knowledge would in turn, be helpful in using bands as kinematic indicators of silicic dome emplacement and for determining strain.

Banding in silicic lavas can arise from a number of distinct syneruptive mechanisms, including mixing of chemically distinct magmas (e.g., Gibson and Naney, 1992), incorporation and redistribution of xenolithic material in a shear flow (Rust et al., 2004), repeated shear fracturing, healing (RFH) and viscous deformation (Tuffen et al., 2003; Tuffen and Dingwell, 2004), and through juxtaposition and subsequent deformation of texturally distinct magma parcels to form bands (Gonnermann and Manga, 2003). Of these mechanisms, the latter two have something in common in that they call upon a close relationship between the viscoelastic response of silicate melt to flow-related stress, namely, the fracturing-healing processes and the formation of alternating crystal-rich and crystal-poor bands. For example, Gonnermann and Manga (2003) describe a progression of texturally distinct obsidian clasts being stretched by shear flow to form bands. They argue that banding is a product of fracturing, displacement, and redistribution and subsequent annealing of texturally heterogeneous magma. A requirement of this model is that magma starts out in a texturally heterogeneous state, although the authors offer no explanation for the causes of initial crystallinity differences. Tuffen et al. (2003) studied the process of band formation in a series of healed fracture zones in conduit obsidian from Iceland. Their observations suggest that textural heterogeneities are a direct result of the fracturing and re-welding processes occurring within the conduit during an eruption. They highlight a feedback between the brittle-ductile deformation process and crystallization of abundant oxide and feldspar microlites in obsidian.

The goal of this paper is to contribute new insights into the mechanism(s) of microlite band formation in obsidian lavas. To this end, we investigate the chemical and thermal histories of flow bands in order to detect whether the crystallinity variations could have arisen from contrasting cooling and degassing paths. We also report on the results of hydrothermal annealing experiments, which simulate the welding process in silicic magma. Our experimental results support the hypothesis that shear-induced fracturing coupled with subsequent reannealing of magma explain the occurrence of flow banding in the examined obsidians (Tuffen et al., 2003). Our conclusions are relevant to understanding the timing and location of flow bands that form in silicic volcanic systems.

METHODS

Samples

Flow banded obsidians were collected from the following late Holocene flows in the western United States: (1) Big Glass Mountain, California, (2) Inyo Domes obsidian, California, and (3) Big Obsidian flow, Oregon. We selected the suite based on the wide range of microlite textures exhibited by these obsidians (Fig. 1) and on their relatively similar calc-alkaline rhyolitic compositions (e.g., Vogel et al., 1989; Eichelberger and Westrich, 1981). The range of samples also reflects that some samples had previously been the subject of earlier phase-equilibrium studies (e.g., Inyo Domes obsidian; Castro and Gardner, 2003) and thus, are well suited for the annealing experiments conducted herein.

All samples come from in-place outcrops near flow perimeters. Obsidians are unaltered and generally devoid of spherulites. Qualitative textural observations were made on doubly polished thin sections of all samples of the collected suite. Big Glass Mountain obsidians form the basis for quantitative textural, calorimetric, and volatile content analysis. Big Glass Mountain obsidians are particularly amenable to these analyses because their microlite abundances are quite low (~1 vol%), thereby reducing the errors on calorimetric measurements and dilution effects on Fourier transform Fourier transform infrared spectroscopy (FTIR) analyses. Textural measurements were performed according to the method of Castro et al. (2003), which yields the crystal size distribution (CSD) in terms of length (l) and width (w), the number density (N_V), and volume percent of pyroxene (Px) crystals.

Analytical

H_2O concentrations were determined on doubly polished Big Glass Mountain obsidian wafers ranging from 49 to 220 μm. Wafer thickness was determined with a Mitutoyo digital gauge, with a precision of ±2 μm. Infrared spectroscopic measurements were performed on a Thermo Nicolet Magna 760 FTIR spectrometer interfaced with a NicPlan infrared (IR) microscope at the Lawrence Berkeley Lab Synchrotron Infrared Science Facility (beamline 1.4.3). Transmittance spectra were obtained over the mid-IR (1400–4000 cm^{-1}) to the near-IR (3700–6500 cm^{-1}) regions with Mercury Cadmium Telluride detectors, KBr beam splitters, and the synchrotron light source. Between 500 and 1024 scans were used to obtain each spectrum. Each obsidian wafer was analyzed 2–10 times, with spots positioned along linear traces within texturally distinct bands. Due to low dissolved H_2O contents (typically <1 wt%) in many obsidians, we encountered low signal-to-noise ratios for absorption bands 4500 cm^{-1}

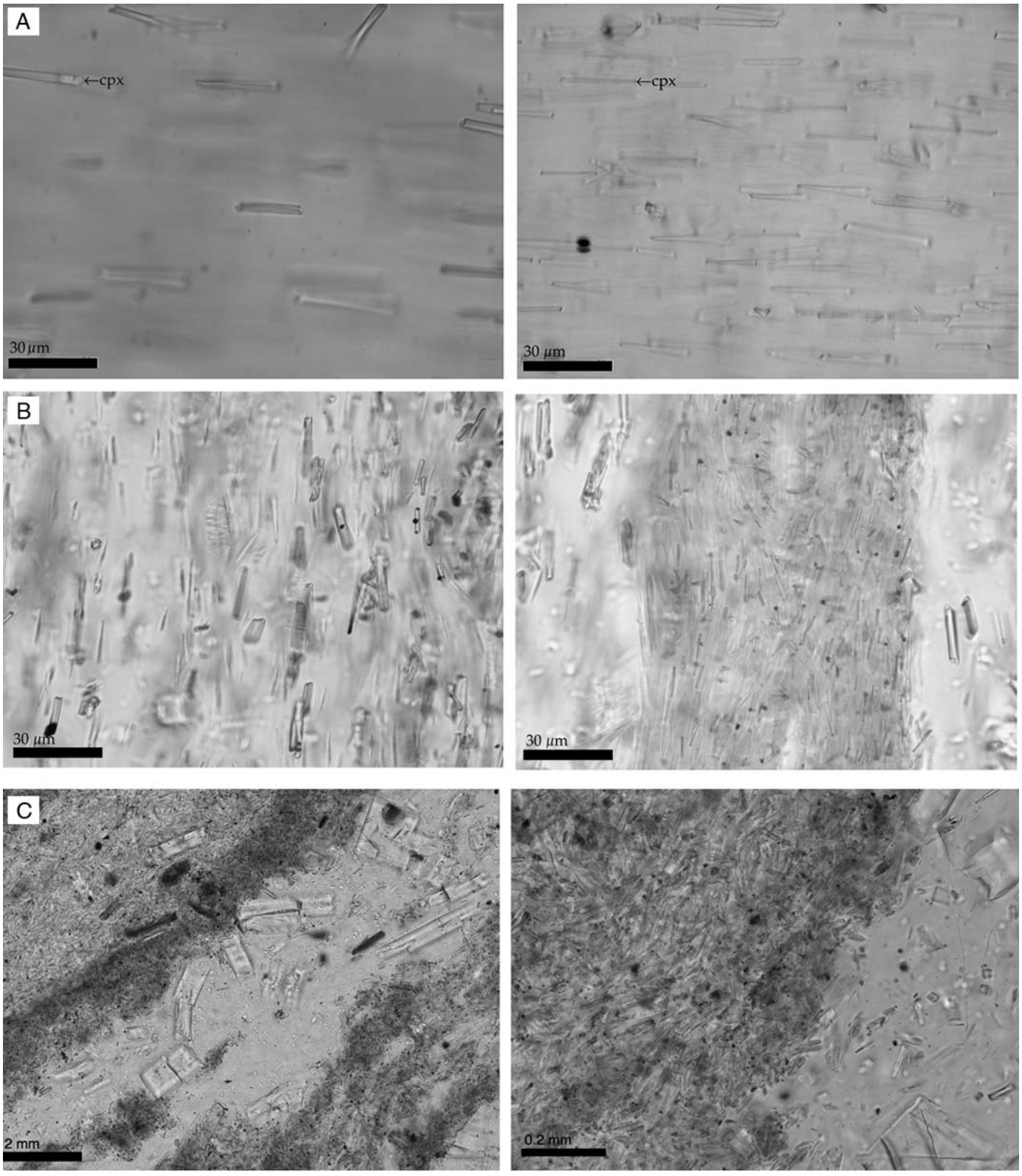

Figure 1. Photomicrographs of microlite-defined flow banding in various obsidian from Big Glass Mountain (A), Big Obsidian flow (B), and the Inyo Domes (C). Images on the left highlight microlite-poor bands, while those on the right show microlite-rich bands (cpx—clinopyroxene).

and 5200 cm^{-1}, corresponding to dissolved OH^- groups and molecular H_2O, respectively (Stolper, 1982). In these cases, total H_2O concentrations were determined from the intensity of the 3750 cm^{-1} absorption band, utilizing absorption coefficients of Ihinger et al. (1994).

Calorimetric measurements were made on two obsidian samples (BGMx1, BGMx2) in order to determine the glass transition temperatures (T_g) and quantify cooling rates of microlite-rich and microlite-poor bands via relaxation geospeedometry (Dingwell, 1995). Samples consisted of 6-mm-diameter cylinders of Big Glass Mountain obsidian drilled from microlite-rich and microlite-poor bands spaced ~1 cm apart. Cylinders were ~2 mm in length. Materials were cleaned in ethanol and dried in a vacuum oven prior to loading in the calorimeter.

Calorimetric measurements were performed on a NETZSCH ® Differential Scanning Calorimeter (DSC) 404C Pegasus at the University of Munich. The constant pressure heat capacity (C_p) of each sample was measured to ~50 K above the glass transition at a heating rate of, firstly, 5 K min^{-1}, then subsequently at 20, 15, 10, and 5 K min^{-1} after cooling at a matching rate. For each case, in the glass state the C_p follows a temperature-dependent path (Fig. 2). The glass transition interval is defined by a peak in C_p. In physical terms, the glass transition interval is the temperature interval over which a melt changes from liquid-like (e.g., ductile or visco-elastic response to stress) to solid-like (e.g., brittle response to stress) behavior. The temperature at which the maximum in the peak occurs has been used here to define a single glass transition temperature (T_g) for a given cooling and heating rate. At temperatures above the glass transition interval, the glass converts to a supercooled liquid state in which the melt structure is completely relaxed. This state is characterized by relatively constant C_p values with increasing temperature (Fig. 2). Following the Tool-Narayanaswamy approach (Narayanaswamy, 1971, 1988) these curves were then used to determine the natural cooling rates of the bands following the modeling procedure described in detail by Wilding et al. (1995) and Gottsmann and Dingwell (2001). The C_p curves measured for known matching cooling and heating rates are modeled in order to provide a set of sample-specific parameters (Table 1). These parameters then enable the C_p curve determined during the initial heating to be modeled, in order to define the natural cooling rate across the glass transition.

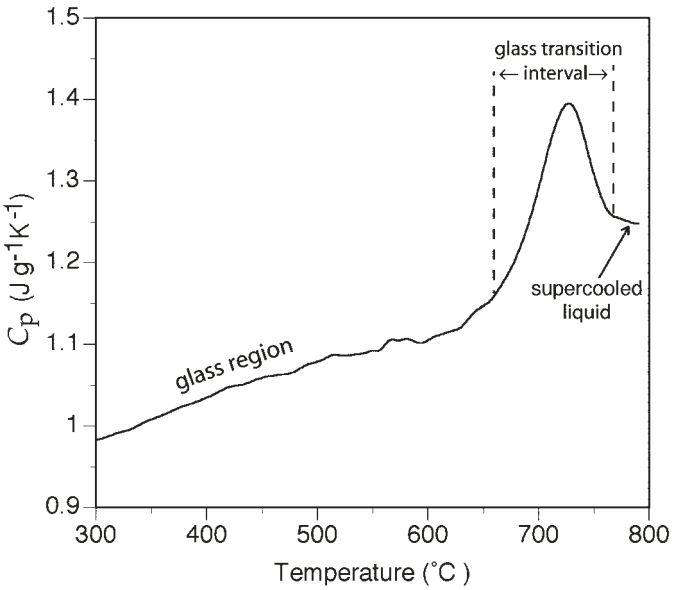

Figure 2. Raw heat capacity (C_p) curve for sample BGMx2. Curve was generated by heating the sample in a calorimeter at 5 K min^{-1} to ~50 K into the supercooled liquid field. The curve is characterized by three zones: glass state, glass transition interval, and supercooled liquid field. The glass transition temperature (T_g) is defined by the peak in the heat capacity trace.

TABLE 1. FIT PARAMETERS AND MODELED COOLING RATES FOR BIG GLASS MOUNTAIN (BGM) OBSIDIANS

Sample	H_2O	$\log_{10}$ A (s)	ΔH (kJ mol^{-1})	ξ	β	T_g (°C)	Cooling rate (K min^{-1})
BGMx1	0.13	–13.6	303	0.98	0.97	739	0.01
BGMx2	0.13	–14.3	312	1.0	0.90	731	0.02

Experimental

Hydrothermal annealing experiments were conducted on Inyo Domes obsidian, collected from a pyroclastic deposit adjacent to Obsidian Dome, California. This unaltered glassy rhyolite contains ~5% microphenocrysts of plagioclase, biotite, hornblende, and quartz. Microlites of pyroxene (Px), oxide (Ox), biotite, and feldspar (Kfs) occupy ~1–30 vol% of the groundmass. The major element composition of the Inyo rhyolite is published in Castro and Mercer (2004). The obsidian was ground with an agate mortar (~100–500 µm), rinsed in ethanol, and dried in a desiccation chamber. Approximately 0.05 g of starting material was loaded into 3-mm-diameter Au capsules with enough distilled water to ensure water saturation at the pressure-temperature conditions. Au capsules were then sealed by crimping, weighed, and then welded shut with an oxy-acetylene torch. Welded capsules were heated for ~10 min and re-weighed to verify that no water was lost.

Experiments were performed at the University of Alaska, Fairbanks, in Rene-style, externally heated, cold-seal pressure vessels with nickel filler rods and H_2O as the pressurizing fluid. The experimental configuration fixes the oxygen fugacity at 0.5–1 log units above the NNO buffer (Geschwind and Rutherford, 1995; Gardner et al., 1995). Pressure was monitored with an electronic pressure transducer with a precision of ±0.5 MPa. Some of the pressure vessels were fitted with rapid quench extensions, wherein molten samples are immersed in a water-cooled jacket at the base of the vessel. Quench rates in these vessels are on the order of 150 °C s^{-1}, and thus samples cool below their

glass transitions in ~2–3 s (Gardner et al., 2000). Experiments performed in non-rapid-quench pressure vessels were initially quenched with compressed air, followed by immersion of the vessel in a water bath. We estimate quench times in these experiments to be on the order of 1–2 min. Temperature was measured with K-type (chromel-alumel) thermocouples, precise to ±4 °C, with accuracy determined by B-type thermocouples calibrated at the melting point of gold (Gardner et al., 2000).

All annealing experiments were run under H_2O-saturated conditions ($P_{H2O} = P_{total}$). We performed experiments by bringing the starting material directly to *P-T* conditions within a period of ~0.5 h. Charges were then subjected to fixed *P* (50 or 100 MPa) and *T* for 7 d. The experimental temperatures (~750–850 °C) were guided by estimates of eruption temperature from mineral geothermometry (Vogel et al., 1989; Gibson and Naney, 1992), whereas pressures of 50 and 100 MPa were chosen to be consistent with the range of magmatic H_2O contents (~3–4 wt%) measured on melt inclusions in the Inyo rhyolite (e.g., Hervig et al., 1989).

At the conclusion of each experiment, capsules were cleaned in an ultrasonic bath and dried. Capsule deformation occurred in all experiments, and was indicated by irregular flattening and folding of the Au tubing. It is difficult to quantify the strain recorded in quenched experimental charges, as some of the deformation is partitioned into compaction of the starting powder and then into viscous deformation once the charge is molten. Nonetheless, we infer that the capsules experienced pure shear, as the experimental setup transmits hydrostatic pressure, and we estimate the pure shear strains to be between 0.5 and 1, based on the deformation of tubes and comparison of pre- and post-run sample volumes. Comparison of pre- and post-run weights ensured that charges remained sealed during the experiment. The presence of water upon piercing the charge provided additional evidence that the capsules lost no water during the experiment. Annealed glass was removed by dissecting the Au capsules and subsequently mounting the charge on a glass slide, which was later polished for microscopic imaging.

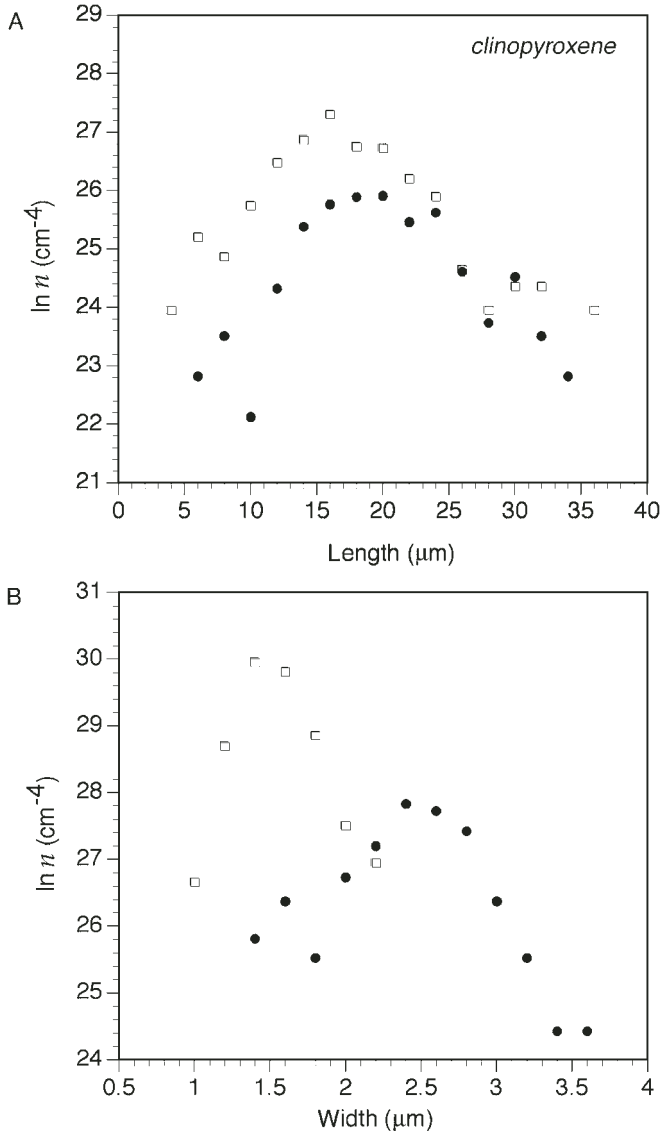

Figure 3. Crystal size distributions of Px in microlite-rich (open squares) and microlite-poor (solid circles) bands. The vertical axis indicates the natural log of the population density (*n*), or the number of microlites per volume per unit length. Note that the modal length is greater in microlite-poor bands, whereas the number density of crystals is higher by 1–2.5 orders of magnitude in the microlite-rich bands. These textural trends also hold for oxide and feldspar microlites.

RESULTS

Band Textures

Figure 1 shows representative flow band textures from three rhyolitic obsidian flows. Mineralogy amongst bands is comparable, consisting of Px, Ox, and Kfs, however, the crystal size and number density vary systematically for each mineral phase. The general observation is that microlite-rich bands have textures having higher N_V and smaller modal length (*l*), as illustrated, for example, by Px (Fig. 3). By contrast, microlite-poor bands have textures containing fewer microlites with larger average and modal *l*. All microlite phases exhibit these patterns. Figure 3A shows crystal size distributions for Px in microlite-rich and microlite-poor bands in Big Glass Mountain obsidian. Length and width distributions are log normal in both bands, as determined by chi-squared analysis (Eberl et al., 2002). Length distributions follow the pattern of widths, showing higher modal *l* in microlite-poor bands. Differences in modal width (Fig. 3B) are pronounced and indicate smaller modal width in microlite-rich layers compared to microlite-poor counterparts.

In addition to the size distribution differences, bands also display a systematic contrast in oxide concentration. Microlite-rich bands always contain higher abundances of Ox (predominantly magnetite) than microlite-poor bands. Glass color also correlates with band crystallinity. In particular, microlite-rich bands in Big

Obsidian flow and Inyo Domes obsidians often show a reddish hue in plane polarized light. This color is interpreted to be the result of submicroscopic hematite "nanolites" (Sharp et al., 1996) in the glass.

Volatile Contents

All Big Glass Mountain obsidians contain low volatile concentrations, having on average 0.13 ± 0.01 wt% H_2O. Such low values are consistent with degassing during shallow ascent and near-surface extrusion (Eichelberger et al., 1986). Figure 4 shows H_2O contents of Big Glass Mountain obsidians determined by FTIR after correcting for the vol% of microlites. Both microlite-rich and microlite-poor bands contain less than 0.15 wt% H_2O, however microlite-poor bands show a lower minimum H_2O content (0.11 wt%). This variation in H_2O contents is greater than analytical error (±10% relative). Despite this variation, it is hard to confirm that differences between H_2O content correlate to the microlite content in bands, because the small number of analyses does not permit a statistical interpretation.

Thermal Analysis

The glass transition temperature (T_g) and cooling rates of microlite-rich (BGMx1) and microlite-poor obsidians (BGMx2) are listed in Table 1. Results are also reported in the form of heat capacity traces, shown in Figure 5, which were produced by heating each sample at a rate of 5 K min^{-1} across the glass transition interval. T_g values, shown by the peak in the C_p trace (Fig. 5A), of BGMx1 (739 ± 3 °C) and BGMx2 (731 ± 3 °C) bands are similar. Also notable is the close correspondence between C_p peak heights; some of the offset in C_p curves is related to slightly different sample masses and geometries. Collectively, these observations imply that the samples had similar cooling histories. The higher T_g obtained for sample BGMx1 may suggest a slightly faster cooling rate than BGMx2. The relation between cooling rate and T_g is illustrated in Figure 5B, which shows C_p traces derived from thermal treatments of matched cooling and heating rates of 20, 15, 10, and 5 K min^{-1} for sample BGMx1. Peak positions in these C_p traces increase by more than 30 K from matched cooling and heating rates of 5 to those of 20 K min^{-1}. Further evidence of slow natural cooling rates is provided by the higher glass transition peak generated on initial heating compared to those of the matched cooling and heating rates (Fig. 5B; Gottsmann and Dingwell, 2001).

Figure 6 shows the results of modeling of C_p traces derived from first heating (5 K min^{-1}) of microlite-rich (BGMx1) and microlite-poor bands (BGMx2). In each plot, a best-fit curve is shown that approximates the evolution of the "raw volcanic" heat capacity as a result of structural relaxation in the glass transition (Wilding et al., 1995). Model parameters that govern the goodness of fit to the raw data are shown in Table 1. Cooling rates implied by these fits are 0.01 K min^{-1} and 0.02 K min^{-1} for microlite-rich (BGMx1) and microlite-poor (BGMx2) bands, respectively. We estimate that these values fall within the experimental error of the measurements, and thus it appears that cooling rates are indistinguishable between microlite-rich and microlite-poor bands.

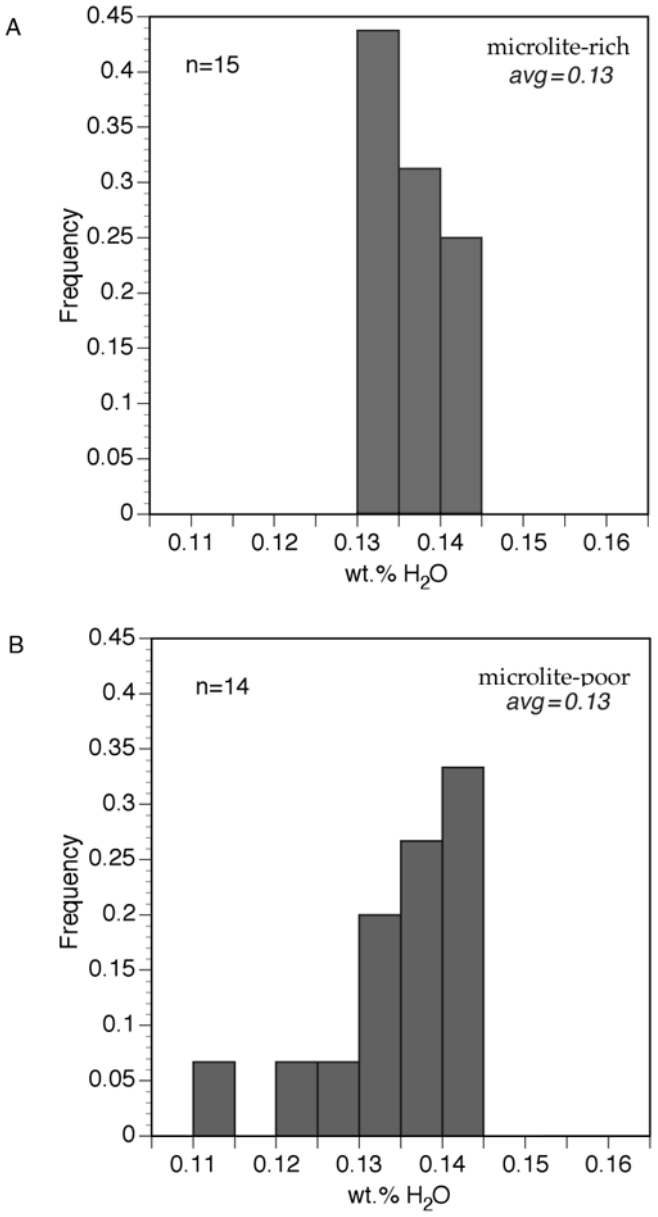

Figure 4. Histograms of H_2O content for microlite-rich (A) and microlite-poor (B) bands. While average H_2O contents are equal for both samples (~0.13 wt%), the distribution in microlite-poor bands shows a tail to lower H_2O contents.

Annealing Experiments

Results of annealing experiments are shown in Figure 7 as a series of photomicrographs collected from experimental charges produced at various *P-T* conditions. In the 50 MPa experiments,

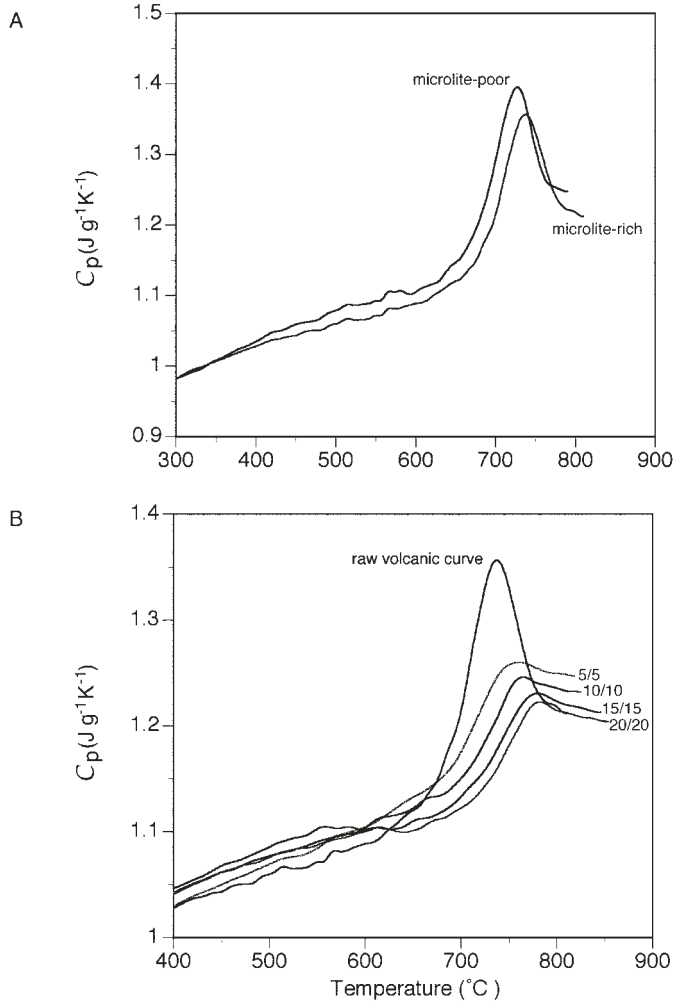

Figure 5. (A) Heat capacity (C_p) traces measured by differential scanning calorimetry (DSC) for two Big Glass Mountain flow bands spaced ~2 cm apart (BGMx1, BGMx2). Upper black curve (BGMx1) was determined on a microlite-poor band, while the lower dark-gray (BGMx2) curve represents a microlite-rich band. Similarity in curve forms implies similar cooling histories across the glass transition. Note the close correspondence of glass transition temperatures, defined here as the peak in the C_p trace. (B) C_p curves for BGMx1, showing the curve produced for the volcanic glass on first heating (at 5 K min^{-1}) and curves produced in matched heating and cooling cycles. C_p curves of thermal treatments of 20, 15, 10, and 5 K min^{-1} (labeled) show a systematic shift in glass transition temperature.

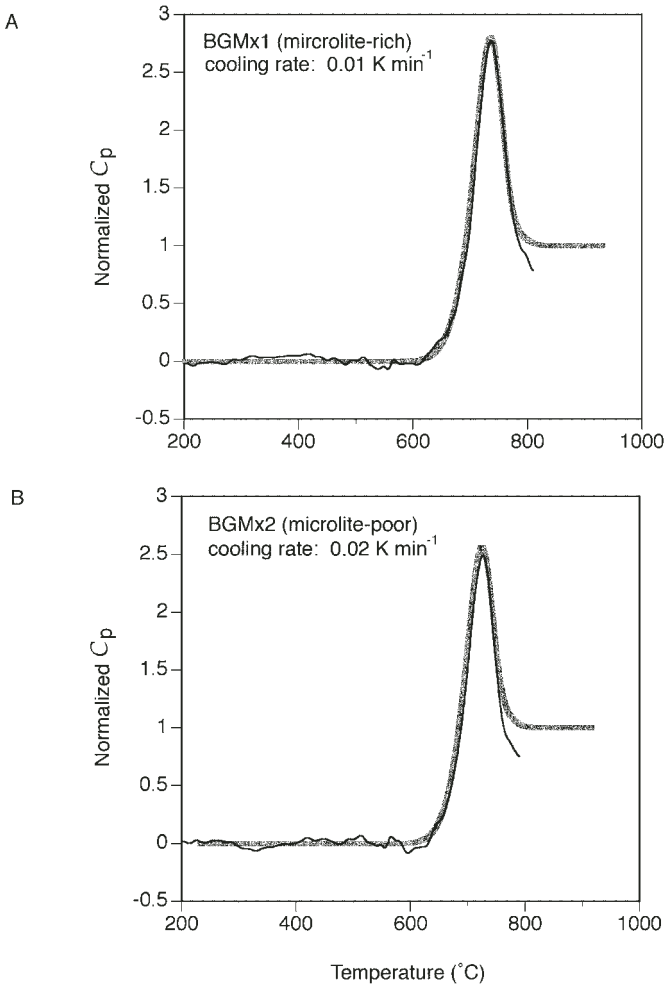

Figure 6. Normalized heat capacity (C_p) traces for two Big Glass Mountain flow bands (BGMx1, BGMx2). Bold gray curves are the model fits to the C_p traces that allow the cooling rate across the glass transition to be determined (Wilding et al., 1995). Both bands yield relatively slow cooling rates, and, despite sharp textural differences, cooling histories did not differ significantly between these bands.

lower temperature runs (750–800 °C) produced relict grain textures (from powdered starting materials) characterized by angular fragments and fine-grained oxide coatings that accentuated the grain boundaries. Larger glass fragments (>100µm) also appeared to contain abundant newly formed Kfs microlites. Kfs and Ox microlites are expected to form due to their saturation in the Inyo melt at these experimental conditions (Castro and Gardner, 2003). The textural characteristics (N_V and size) of Kfs microlites are qualitatively similar to those observed on microlite-rich Inyo Domes obsidian flow bands (Fig. 1C). Fine-grained, annealed powder fills the space between larger fragments and often appears darker due to locally high concentrations of oxides and a reddish hue that we attribute to the presence of hematite in the glass (Fig. 7A). Apparently, the increased surface area of matrix regions promotes crystallization. Grain boundary oxide coatings remain intact after all finer grained matrix has annealed (Fig. 7B). At 850 °C and 50 MPa, relict grain textures appear to give way to more homogeneous textures typified by parallel and curved stringers of oxides, which in many respects resemble natural flow bands (Fig. 7C). The small flow bands deflect around vesicles and microphenocrysts. Clearly, viscous flow occurred within the charge at 850 °C, and the flow was likely to have been induced by deformation of the experimental capsule.

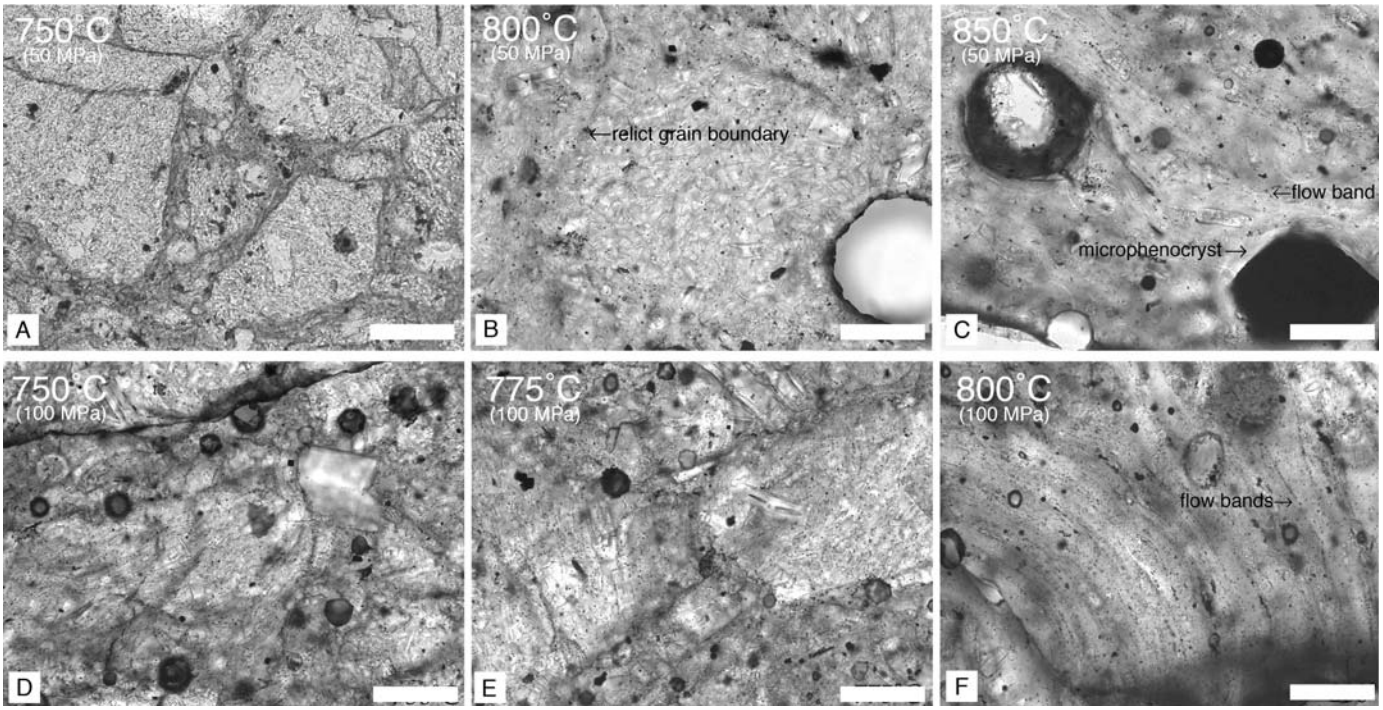

Figure 7. Plane light photomicrographs (200×), showing textures produced in annealing experiments. Scale bars are 100 μm long. (A–C) Experiments conducted at P_{H2O} = 50 MPa and a range of temperatures. Relict granular texture is evident at 750 °C. Intergranular matrix consists of finely ground, reddish-brown glassy powder, oxide (Ox; black grains), and feldspar (Kfs) microlites (not discernable at given scale). Large grains consist of relatively colorless glass with abundant Kfs and Ox microlites. Grain boundaries at 800 °C are evidenced by strings of Ox grains, although they are less distinct. At 850 °C, all grain boundaries are erased and viscous flow occurs resulting in aligned microlites and flow bands defined by Ox trains. (D–F) Textures at P_{H2O} = 100 MPa show a similar progression of relict grain boundaries (750–775 °C) followed by complete erasure of those boundaries at 800 °C. Flow bands, again defined by oxide trains, are very well developed at 800 °C.

We find that the point at which relict grain boundaries are erased shifts to lower temperature at higher P_{H2O}. In 100 MPa experiments, relict grain textures persist until ~775 °C (Fig. 7E). Beyond this temperature, the grain boundaries become diffuse and are eventually totally undetectable. Above 800 °C, the melt apparently deformed by way of viscous flow, again in response to deformation of the capsule. As was seen in the 50 MPa experiments, flow bands defined by trails of oxides were also produced at 100 MPa, albeit at the lower temperature of 800 °C (Fig. 7F).

We interpret these experimentally produced flow bands as the vestiges of grain boundary oxide coatings and the locally enriched matrix oxides that underwent deformation during viscous flow at high temperature. Given our estimates of total pure shear strains of ~0.5–1 for these small (<0.5 cm) experimental charges, we suggest that bands could be developed over relatively short (<1 cm) length scales and for small strains.

DISCUSSION

We investigated the thermal and chemical history of microlite-defined flow bands in obsidian in order to place further constraints on their mode of origin. Of the existing models of band production, our experimental results support the models of Tuffen et al. (2003) and Gonnermann and Manga, (2003), which postulate that flow bands are a direct product of viscoelastic deformation processes in the melt during flow in the conduit. Our experiments simulate "healing" part of the RFH process of Tuffen et al. (2003), in that we subjected fragmented melts to P_{H2O}-T conditions sufficient to fully anneal and drive viscous deformation in the material. Such experiments provide the first experimental proof that bands can develop as a result of the fracture-annealing-flow processes in silicic melt. Our calorimetric and volatile content analyses provided further tests on other triggers for microlite crystallization in obsidians that were not addressed by the models of Tuffen et al. (2003) and Gonnermann and Manga (2003), namely, the influences of conductive cooling rate and degassing on band formation. Below, we discuss the salient findings of our chemical, thermal, and experimental analyses.

Volatile content data and textural observations reveal no correlation between microlite content and volatile content; equally degassed obsidians may have either microlite-rich or microlite-poor textures. This fact suggests that microlite abundances and size distributions are not a function of the total amount of H_2O liberated. The degassing path, or rate of gas loss, may however differ for microlite-rich and microlite-poor flow bands and, thus, may be responsible for the sharp contrast in texture.

Relationships between degassing path and crystallization behavior have been determined experimentally for H_2O-saturated rhyolite melts undergoing isothermal decompression (e.g., Hammer and Rutherford, 2002). Such studies show that large chemical undercoolings resulting from rapid degassing lead to abundant microlite nucleation. In this regime, nucleation, as opposed to growth, dominates as the primary crystallization mechanism. Alternatively, under conditions of slow steady degassing, a growth-dominated crystallization regime may govern crystal populations, resulting in fewer yet larger crystals. Therefore, while the final H_2O contents of variably crystalline obsidians may be uniformly low, their degassing paths could have been quite different. We interpret microlite-rich bands as recording relatively larger undercoolings than microlite-poor bands, by virtue of their higher N_V and smaller modal crystal size (Fig. 3). Conditions that would foster rapid degassing and abundant microlite nucleation include the formation of fracture networks and related regions of high permeability that aid in gas escape (Tuffen et al., 2003; Rust et al., 2004). The formation of a fracture in an otherwise dense melt will lead to a local pressure drop, and potentially, a large pressure gradient. Rapid degassing of the melt immediately surrounding fractures could lead to microlite-enriched zones adjacent to microlite-poor zones, where the melt volatile contents remain higher (Fig. 8).

Calorimetric measurements yield information on the cooling histories of obsidians immediately prior to quenching. That is, the calculated cooling rates and measured T_g values apply only to the latest passage of the melt through the glass transition. Because we find only negligible differences in T_g and cooling rate between microlite-rich and microlite-poor bands, we conclude that the latest stage of cooling across the glass transition (i.e., quenching at flow cessation) probably did not cause the development of crystal-rich and crystal-poor layers. In other words, microlite banding probably did not originate during the emplacement of these flows. Textural differences may still reflect diverse cooling histories in the conduit, however, we cannot resolve these complexities with the calorimetric approach. Nonetheless, calorimetric measurements suggest that, if flow bands arose from fragmentation followed by subsequent annealing and deformation of fragments, both microlite-rich and microlite-poor materials would reach thermorheologic equilibrium with one another during extrusion on the surface and experience a common final cooling path.

Aspects of the welding process were simulated in hydrothermal annealing experiments on Inyo Domes obsidian, and such experiments provide insights into the time scales, requisite strains, and pressure-temperature conditions related to flow band formation. We estimate that all experiments were conducted above T_g, based on earlier calorimetric measurements on the compositionally similar Big Glass Mountain obsidian (Table 1; Eichelberger and Westrich, 1981) and the high H_2O contents of the experimental melts (~3–4 wt%), which reduce T_g by several tens to more than 100 °C. Microlite crystallization took place in all experiments due to fact that experimental

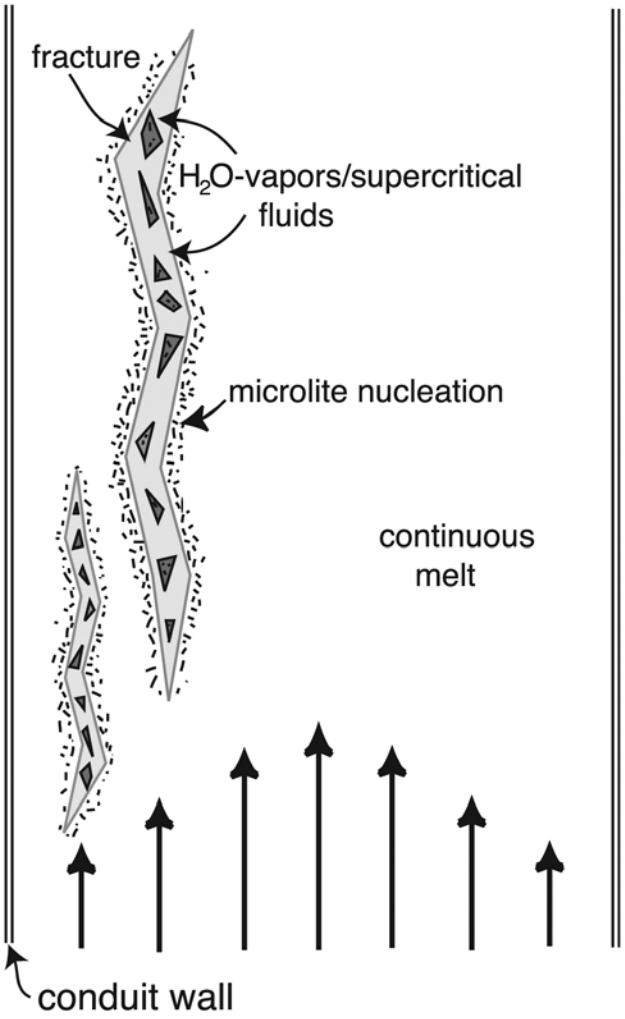

Figure 8. A schematic diagram showing the conditions leading to shear fragmentation, degassing, and microlite crystallization in silicic magma within a conduit (e.g., Tuffen et al., 2003). Bold arrows show flow velocity profile. Microlite content heterogeneities may be created in regions of localized decompression and degassing in the vicinity of fractures. Subsequent annealing and flow preserves these heterogeneities as flow bands. Diagram is not to scale.

P-T conditions positioned the melts well within the Ox and Kfs stability regions for the Inyo starting composition (Castro and Gardner, 2003). In both 50 and 100 MPa experiments, textures progressed from relict-fragmental to banded textures lacking discernable grain boundaries (Fig. 7). These changes occurred with increasing temperature at both pressures. Notably, the temperature at which banding is produced increases with declining P_{H2O}, reflecting the strong influence of H_2O content on melt viscosity and hence diffusion time scales in the silicate melt. Thus, at lower P_{H2O}, the annealing process will take longer at a fixed temperature than at high P_{H2O}. Experimental time scales of ~7 d were sufficient to produce flow bands in the highest

temperature runs (800–850 °C). We interpret this one-week time scale to be a maximum at these high-T conditions, because it is possible that the bands formed on shorter time scales and remained undetected until the conclusion of the experiments. At lower temperatures, grain boundaries remained intact, suggesting that longer run times would lead to eventual erasure of these boundaries and possible flow of the melt. Time scales greater than about one week may therefore be required to produce flow bands at lower T (<800 °C) and P_{H2O} (<50 MPa) conditions.

The relatively static nature of the experiments (P = hydrostatic) undoubtedly differs from the true conduit-flow environment, where deviatoric stresses would potentially aid in band formation, mainly through the production of viscous heat (e.g., Polacci et al., 2001) and, in melts undergoing shear-induced fragmentation, frictional heating (Tuffen and Dingwell, 2004). Viscous and frictional heating would potentially buffer the effects of conductive cooling and adiabatic expansion of degassed vapors and in so doing, reduce the time required to fully anneal and generate bands. Therefore, in natural conduits, we would expect that progressive degassing would inhibit band formation while continued shearing would offset this effect, leading to shorter banding time scales. To date, our experimental observations are too few to provide bracketing values on the time scales of band formation.

Experimental banding textures are the result of redistribution of oxide grains by viscous flow in experimental capsules, driven by small capsule deformations and aided by reduced viscosities of high-temperature melts. Given the limited strains (~1) imposed on capsules, we infer that the strains required to form bands from microlite heterogeneities may be quite small. This observation, in turn, implies that the dimensions of natural bands, particularly their thickness, are not solely a function of the total finite strain imposed but also the size and geometry of the initial microlite heterogeneities (e.g., grain boundary coatings). In other words, the dimensions of bands may be as much a consequence of the size of fracture zones and their geometry as they are the amount of strain (Tuffen and Dingwell, 2004). Therefore, the use of band dimensions as a measure of finite strain may not be warranted.

CONCLUSIONS

We examined the chemical and physical aspects of flow bands in obsidians in order to better constrain their mode and location of origin. In addition, we performed experimental simulations of the annealing process in silicic melt to identify the controlling factors in band formation and to estimate time scales over which these features form. The primary conclusions of this study are as follows:

1. Chemical (H_2O) and thermal analyses, although insensitive to the early complex cooling and degassing paths of obsidians, suggest that microlite heterogeneities could not have formed during cooling and degassing at the time of extrusion and must have originated in the conduit.

2. Annealing experiments show that microlite (primarily oxide) heterogeneities may develop in fractured regions of silicic melt that are saturated in an H_2O-rich vapor phase. Deformation of these heterogeneities to form flow bands may occur on time scales of ~7 d or less, provided the melt is sufficiently hot and being sheared.

3. Pure shear strains of ~1 are sufficient to produce banding in annealed fragments. We note that the dimensions of bands (e.g., thickness) may not be a reliable indicator of finite strain in obsidians, because band dimensions are likely determined by the breadth of fracture zones and related crystallization zones. We suggest then, that the geometric characteristics of bands cannot be used as an indicator of finite strain, although their local distortions around inclusions (e.g., crystals and bubbles) may be used to make inferences on flow kinematics (see Manga, this volume).

ACKNOWLEDGMENTS

The authors thank H. Gonnermann and K. Russell for their constructive reviews and M. Manga for comments. H_2O analyses were facilitated by M. Martin of the Advanced Light Source at Lawrence Berkeley National Laboratory. J. Castro is grateful for the generous support of the Alexander von Humboldt Foundation and the Deutscher Akademischer Austausch Dienst. Experimental work was made possible by National Science Foundation (NSF) grants EAR-0106658 and EAR-0400745 to J. Larsen and J. Gardner.

REFERENCES CITED

Castro, J.M., and Gardner, J.E., 2003, Phase equilibria and kinetic crystallization experiments on the Inyo Domes rhyolite: Eos (Transactions, American Geophysical Union), v. 84 (46).

Castro, J.M., and Mercer, C., 2004, Microlite textures and volatile contents of obsidian from the Inyo volcanic chain, CA: Geophysical Research Letters, v. 31, p. L18605, doi: 10.1029/2004GL020489.

Castro, J.M., Cashman, K.V., and Manga, M., 2003, A technique for measuring 3D crystal-size distributions of prismatic microlites in obsidian: The American Mineralogist, v. 88, p. 1230–1240.

Dingwell, D.B., 1995, Relaxation in silicate melts: Some applications, *in* Stebbins, J., et al., eds., Structure, dynamics and properties of silicate melts: Reviews in Mineralogy, v. 32, p. 21–66.

Eberl, D.D., Kile, D.E., and Drits, V.A., 2002, On geological interpretations of crystal size distributions: Constant vs. proportionate growth: The American Mineralogist, v. 87, p. 1235–1241.

Eichelberger, J.C., and Westrich, H.R., 1981, Magmatic volatiles in explosive rhyolitic eruptions: Geophysical Research Letters, v. 8, p. 757–760.

Eichelberger, J.C., Carrigan, H.R., Westrich, H.R., and Price, R.H., 1986, Non-explosive silicic volcanism: Nature, v. 323, p. 598–602, doi: 10.1038/323598a0.

Gardner, J.E., Rutherford, M., Carey, S., and Sigurdssson, H., 1995, Experimental constraints on pre-eruptive water contents and changing magma storage prior to explosive eruptions of Mount St. Helens volcano: Bulletin of Volcanology v. 57, p. 1–17.

Gardner, J.E., Hilton, M., and Carroll, M.R., 2000, Bubble growth in highly viscous silicate melts during continuous decompression from high pressure: Geochimica et Cosmochimica Acta, v. 64, p. 1473–1483, doi: 10.1016/S0016-7037(99)00436-6.

Geschwind, C., and Rutherford, M.J., 1995, Crystallization of microlites during magma ascent: The fluid mechanics of recent eruptions at Mount St. Helens: Bulletin of Volcanology v. 57, p. 356–370.

Gibson, R.G., and Naney, M.T., 1992, Textural development of mixed, finely porphyritic silicic volcanic rocks, Inyo Domes, eastern California: Journal of Geophysical Research, v. 97, p. 4541–4559.

Gonnermann, H., and Manga, M., 2003, Explosive volcanism may not be an inevitable consequence of magma fragmentation: Nature, v. 426, p. 432–435, doi: 10.1038/nature02138.

Gottsmann, J., and Dingwell, D.B., 2001, Cooling dynamics of spatter-fed phonolite obsidian flows on Tenerife, Canary Islands: Journal of Volcanology and Geothermal Research v. 105, p. 323–342, doi: 10.1016/S0377-0273(00)00262-6.

Hammer, J.E., and M.J., Rutherford, 2002, An experimental study of the kinetics of decompression-induced crystallization in silicic melt: Journal of Geophysical Research, v. 107, ECV8-1-ECV-24, doi: 10.1029/2001JA900144.

Hervig, R.L., Dunbar, N.W., Westrich, H.R., and Kyle, P.R., 1989, Pre-eruptive water content of rhyolitic magmas as determined by ion microprobe analyses of melt inclusions in phenocrysts: Journal of Volcanology and Geothermal Research, v. 36, p. 293–302.

Ihinger, P.D., Hervig, R.L., and McMillan, P.E., 1994, Analytical methods for volatiles in glasses, *in* Carroll, M.R., and Holloway, J.R., eds., Volatiles in magmas: Reviews in Mineralogy, v. 30, p. 67–121.

Narayanaswamy, O.S., 1971, A model of structural relaxation in glass: Journal of the American Ceramic Society, v. 54, no. 10, p. 491–498.

Narayanaswamy, O.S., 1988, Thermorheological simplicity in the glass transition: Journal of the American Ceramic Society, v. 71, p. 900–904, doi: 10.1111/j.1151-2916.1988.tb07543.x.

Polacci, M., Papale, P., and Rosi, M., 2001, Textural heterogeneities in pumices from the climactic eruption of Mount Pinatubo, 15 June 1991, and implications for magma ascent dynamics: Bulletin of Volcanology v. 63, p. 83–97, doi: 10.1007/s004450000123.

Rust, A.C., Cashman, K.V., and Wallace, P.J., 2004, Magma degassing buffered by vapor flow through brecciated conduit margins: Geology, v. 32, no. 4, p. 349–352, doi: 10.1130/G20388.2.

Sharp, T.G., Stevenson, R.J., and Dingwell, D.B., 1996, Microlites and "nanolites" in rhyolitic glass: Microstructural and chemical characterization: Journal of Volcanology and Geothermal Research, v. 57, p. 631–640.

Stolper, E.M., 1982, Water in silicate glasses: An infrared spectroscopic study: Contributions to Mineralogy and Petrology, v. 81, p. 1–17, doi: 10.1007/BF00371154.

Tuffen, H., and Dingwell, D.B., 2004, Fault textures in volcanic conduits, evidence for seismic trigger mechanisms during silicic eruptions: Bulletin of Volcanology, v. 67, p. 370–387, doi: 10.1007/s00445-004-0383-5.

Tuffen, H., Dingwell, D.B., and Pinkerton, H., 2003, Repeated fracture and healing of silicic magma generate flow banding and earthquakes?: Geology, v. 31, p. 1089–1092, doi: 10.1130/G19777.1.

Vogel, T.A., Eichelberger, J.C., Younker, L.W., Schuraytz, B.C., Horkowitz, J.P., Stockman, H.W., and Westrich, H.R., 1989, Petrology and emplacement dynamics of intrusive and extrusive rhyolites of Obsidian Dome, Inyo Craters volcanic chain, eastern California: Journal of Geophysical Research, v. 94, p. 17,937–17,956.

Wilding, M., Webb, S.L., and Dingwell, D.B., 1995, Evaluation of a relaxation geospeedometer for volcanic glasses: Chemical Geology, v. 125, p. 137–148, doi: 10.1016/0009-2541(95)00067-V.

Manuscript Accepted by the Society 19 April 2005